RESEARCH ARTICLE

Reconstruction of monsoon evolution in southernmost Sumatra over the past 35 kyr and its response to northern hemisphere climate changes

Shengfa Liu[1,2]* , Hui Zhang[1], Xuefa Shi[1,2]*, Min-Te Chen[1,2,3], Peng Cao[1], Ziye Li[4], Rainer Arief Troa[5], Rina Zuraida[6], Eko Triarso[5] and Hendrizan Marfasran[7,8]

Abstract

Reconstruction of monsoon evolution in the tropical Indian Ocean and evaluation of its influence on large-scale ocean circulation and sea-air interaction processes can help us understand climate driving mechanisms. Herein, we used a gravity core SO184-10043 to present the marine sedimentary record from the southernmost Sumatra, spanning the past 35 kyr. The age model is well constrained by 12 accelerator mass spectrometry (AMS) radiocarbon dates determined in mixed planktic foraminifera. We also measured sediment grain size and major and trace elements to reconstruct the variations in hydrodynamic conditions and chemical weathering intensity. These data were then used to reveal the evolution of the northwest (Indonesian) monsoon system over the past 35 kyr. The results showed that both monsoon current and chemical weathering coincided with summer insolation in the Northern Hemisphere and responded to glacial-interglacial climate changes in the northern Atlantic. Higher grain-size values of sensitive components, increased chemical index of alteration (CIA), and Ba/Sr ratios, together with lower CaO/MgO ratios, reflect a stronger monsoon current and chemical weathering during the late marine isotope stage 3 and Holocene. Higher intensity of chemical weathering might be attributed to a stronger northwest monsoon carrying warm and moist air from the Asian continent to Indonesian waters. Lower values of sensitive components, CIA, and Ba/Sr, along with higher CaO/MgO values, reveal a weaker monsoon current and lower intensity of chemical weathering during the last glaciation-deglaciation phase, which was controlled by a weaker monsoon system. At a millennial timescale, cold events occurred during the following intervals: 30–26 ka BP, Heinrich Stadial 1 (HS1; 18–15 ka BP), Last Glacial Maximum (LGM; 23–18 ka BP), Younger Dryas (YD; 11–10 ka BP), and 8.2 ka BP. The same cold events were identified from core SO184-10043, indicating a perfect match with climatic cooling in the Northern Hemisphere. We also observed periodicities of ~ 7.9 ka, 3.0–3.1 ka, 2.2–2.3 ka, and ~ 1.0 ka in our core records. These periodicities are coincident with solar-induced climate changes and support the hypothesis that monsoon evolution in the tropical Indian Ocean during the late Pleistocene coincided with the climate change in the Northern Hemisphere.

Keywords: Late Pleistocene, Hydrodynamic conditions, Chemical weathering, Indian monsoon, Paleoclimate, Sumatra

* Correspondence: liushengfa@fio.org.cn; xfshi@fio.org.cn
[1]Key Laboratory of Marine Geology and Metallogeny, First Institute of Oceanography, Ministry of Natural Resources, Qingdao 266061, China
Full list of author information is available at the end of the article

Introduction

Monsoonal climate dominates over the northern Indian Ocean, and marine records have revealed its close relationship with global climate changes during the late Pleistocene (Mohtadi et al. 2014; Li et al. 2016). Coastal waters of Sumatra span the equator in the northeastern Indian Ocean and are influenced by seasonal rhythms, i.e., by the southeast Malaysian-Australian monsoon and northwest Indonesian monsoon. These monsoon systems show a biennial alternation between central Asia and Australia (Tomczak and Godfrey 2001; Lückge et al. 2009). During boreal winter (from November to March), the northwest monsoon carries warm and moist air from the Asian continent, causing heavy rainfall over Indonesia in response to the southward migration of the Intertropical Convergence Zone (ITCZ) (Qu et al. 2005). In contrast, precipitation in Indonesia is relatively low between June and September, when the dominant southeast monsoon carries warm and dry air from Australia (Gingele et al. 2002; Spooner et al. 2005; Lückge et al. 2009). Driven by the dominant seasonal monsoon system, the ocean currents along the southernmost coast of Sumatra are highly dynamic in relation to monsoon winds. The northwest monsoon drives the South Java Current (SJC), which is a downstream branch of the Indian Monsoon Current (IMC), and the Equatorial Counter Current (EEC) from the north (Wyrtki 1961; Wijffels et al. 1996). During the southeast monsoon season, the SJC weakens and may even turn back to the west, feeding the South Equatorial Current (SEC) (Wyrtki 1962; Murgese et al. 2008).

To date, most of the monsoon records in the Indian Ocean come from the western side of the South Asian Peninsula, where the abundance of *Globigerina bulloides* represents the intensity of upwelling and serves as an alternative indicator of the rise and fall of the Indian monsoon (Prell and Curry 1981; Kroon et al. 1991; Sijinkumar et al. 2011). In the northeast Indian Ocean, the Bay of Bengal and the Andaman Sea have no evident upwelling activity, but river runoff supplies profuse amounts of freshwater and debris (Kroon et al. 1991; Clemens et al. 1991; Prell et al. 1992; Colin et al. 1999; Dahl and Oppo 2006). Great monsoon changes are often indicated by changes in salinity caused by increased freshwater input, which is reflected in the oxygen isotope values of the planktonic foraminiferal shells (Cullen 1981; Rashid et al. 2007; Mohtadi et al. 2014; Li et al. 2016). A number of recent studies of sediment cores from the southwestern Sumatra showed that upwelling along the islands of Indonesia is significant, and the changes in coastal productivity levels are controlled by monsoon (Li et al. 2016) and the Indonesian Throughflow (ITF) (Xu et al. 2017). The seasonally reversing, open-ocean monsoon currents control the Sumatra coastal sedimentary processes, which are still poorly understood, especially its hydrodynamic conditions and chemical weathering. Moreover, a reliable age model has yet to be put forward.

In this study, we present new sedimentological and geochemical records of well-dated sedimentary archives from the southernmost Sumatra waters spanning the past 35 kyr. Several hydrodynamic conditions and chemical weathering processes are discussed herein to reveal the evolution of the monsoon system during the late Pleistocene. Our goal is to understand the relationship between the local monsoon system, the Northern Hemisphere, and global climate changes.

Material and methods

Gravity core SO184-10043 (07° 18.57′ S, 105° 03.53′ E) with a total length of 382 cm was collected from a water depth of 2171 m at the continental margin off the southernmost Sumatra waters (Fig. 1). The core was taken on a cruise of R/V "Sonne" in August 2005. The core lithology was described in detail after opening the core tube. A total of 74 samples were obtained every 5 cm along the length of the core with a sample depth of 1 cm.

The pre-treatment samples for the grain size analysis were treated with 15 mL of the H_2O_2 solution (30%) to remove organic matter. Afterward, the samples were bathed in 5 mL of the HCl solution (3 mol/L) for 24 h to remove calcareous cements and shell material. All samples were fully desalted and dispersed before the measurements. The sediment grain size was analyzed by Malvern Mastersizer 2000 (UK) at the Key Laboratory of Marine Geology and Metallogeny, Ministry of Natural Resources (MNR), China. Malvern Mastersizer 2000 allows measurements of particle size distribution in the range of 0.02–2000 μm, with a resolution of 0.01 Φ. The error based on repeated measurements was determined to be less than 3%.

Geochemical elements were identified within the sediment samples using an inductively coupled plasma optical emission spectrometer (ICP-OES, Thermo Fisher Scientific iCAP 6300) and inductively coupled plasma mass spectrometer (ICP-MS, Thermo Fisher Scientific X Series II) at the Key Laboratory of Marine Geology and Metallogeny, MNR, China. The homogenized sediment samples were dried in an oven with a temperature of less than 50 °C and were ground to the mesh size of less than 200 mm using an agate mortar. Next, approximately 0.05 g of each sample was dissolved in 1.5 mL of HNO_3 and 1.5 mL of HF at 190 to 200 °C for 48 h, respectively. Then, 50 g of the liquor was prepared for the measurements. The SiO_2, Al_2O_3, Fe_2O_3, MgO, CaO, Na_2O, K_2O, TiO_2, P_2O_5, and MnO contents were measured using ICP-OES, while the Cu, Ba, Sr, V, Zn, Cr, Zr, Pb, Co, and Ni contents were quantified using ICP-MS. The standard sediment reference materials (Chinese National
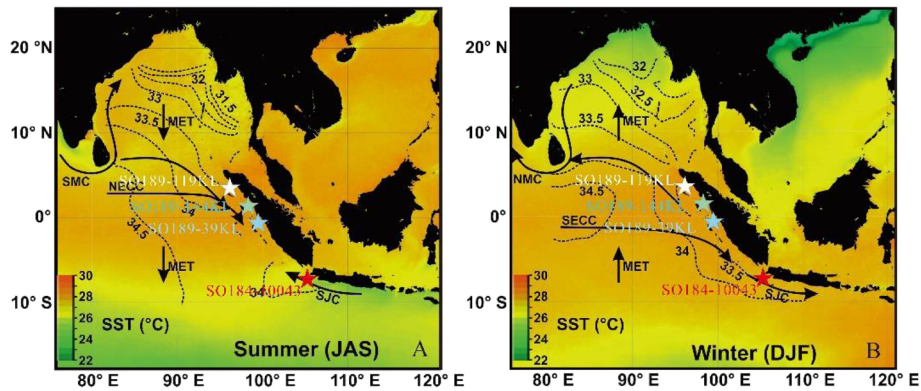
Fig. 1 Location of the sediment core SO184-10043 (red star) with seasonality of surface currents, SST, and salinity in the eastern Indian Ocean (revised from Mohtadi et al. 2014). Seasonal changes in SST (color shading), salinity (dashed lines; psu), and surface currents (arrows) in the study area during boreal summer (top) and winter (bottom). The meridional Ekman transport (ME) is also indicated with arrows. Seasonal SST is averaged for the period between 2002 and 2010 (http://oceancolor.gsfc.nasa.gov/cgi/l3). Salinities are averaged for the period between 1960 and 2004

Standard GSD-9 and GSD-10) and parallel samples were analyzed for quality control. Statistical results showed that relative standard deviations (RSDs) were less than 3% for major elements and less than 5% for trace elements, compared to the previous studies.

AMS^{14}C dating was carried out on 12 samples of mixed planktonic foraminifera (~ 15 mg) (Table 1). Age dating was conducted at the Woods Hole Oceanographic Institution, Massachusetts, USA. Raw AMS^{14}C dates were converted to calendar ages using the CALIB 7.1 and Marine13 calibration curves (Reimer et al. 2013). Local reservoir age ΔR of 42 ± 70 years was chosen for calibration from the online marine reservoir correction database (https://calib.qub.ac.uk/marine) based on the marine reservoir effect of 362 years observed in the Indian Ocean (Southon et al. 2002).

Results

Lithology

Visual inspection of core SO184-10043 indicates that the sediments are composed of olive to dark olive-gray clayey silt. The sediment color, composition, sedimentary structures, and grain size gradually change along the length of the core. For instance, the sediment color changes from olive in the top section (0–105 cm, including some missed length at the top), to olive-gray in the middle section (105–280 cm), and dark olive-gray in the bottom section (280–382 cm). Shell debris and foraminifera were observed at specific intervals (i.e., 34 and 270–370 cm), which coincided with the presence of coarser sandy material. Moreover, two significant tephra layers were identified at 10–12 and 370–382 cm, respectively.

Table 1 AMS^{14}C dating of SO184-10043 determined from planktonic foraminifer *Globigerinoides ruber* shells, and the ^{14}C ages were converted to calendar age by using CALIB7.1 (Reimer et al. 2013)

Lab ID	Depth (cm)	Raw AMS ^{14}C data	Calibrated age (year B.P.)	Mean calibrated age (year B.P.)	Corrected error
OS-112616	25–26	2100 ± 25	1534–1714	1624	± 90
OS-112617	30–31	2380 ± 20	1867–2050	1959	± 92
OS-112618	40–41	2790 ± 20	2349–2575	2462	± 113
OS-112619	95–96	4800 ± 25	4875–5123	4999	± 124
OS-112621	105–106	5110 ± 25	5315–5490	5403	± 88
OS-112622	165–166	7880 ± 30	8217–8373	8295	± 124
OS-112625	180–181	8310 ± 35	8697–8945	8821	± 124
OS-112626	230–231	11,950 ± 55	13,280–13,449	13,365	± 85
OS-112627	240–241	12,950 ± 50	14,488–15,000	14,744	± 256
OS-112628	290–291	18,350 ± 100	21,521–21,854	21,688	± 167
OS-112629	310–311	20,200 ± 120	23,607–23,961	23,784	± 177
OS-112630	350–351	27,700 ± 310	30,995–31,378	31,187	± 192

The changes in core lithology indicate variations in sedimentary environments through time. Considering the current sea level, presence of shells, whelks, and foraminifera, which are characteristics of the marine environment (Qin et al. 1987; Liu et al. 2014), the sediments of core SO184-10043 were likely deposited in a marine environment. Overall, the sediments are distinguished by finer grain size and negligible compositional changes, suggesting a relatively stable depositional environment.

Chronology

Planktic foraminiferal shell samples were collected from 12 sedimentary layers to build the age model for the sediments of core SO184-10043. The dating results showed that the core sediments were accumulated over the past 35 kyr. The sedimentation rates increased gradually up to the present moment and varied between 5 and 29 cm/kyr, with an average of 10 cm/kyr (Table 1). A rapid increase in sedimentation rates is attributed to the flooding of the Sunda Strait in response to global sea-level rise, which might have caused intensified erosion and downslope transport of terrigenous material to the sea (Li et al. 2016). Based on this version of the age model, a sampling interval of 1 cm provided an average resolution of 100 years in this study.
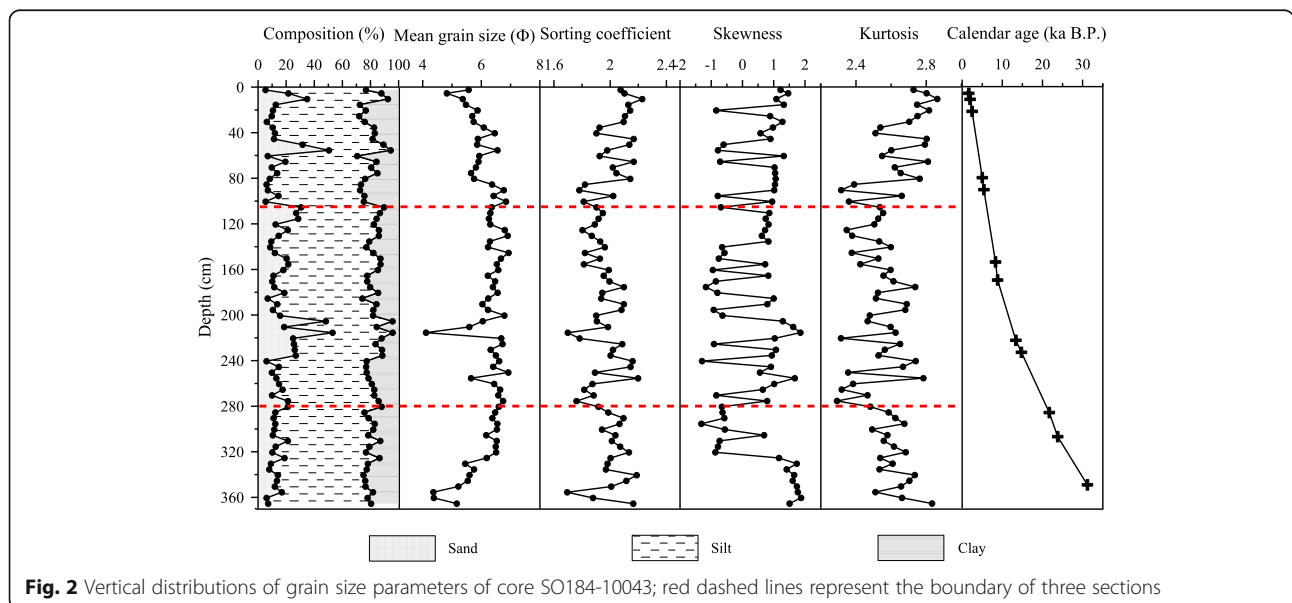
Grain size

We measured the variations in grain size for the sediments of core SO184-10043, including the mean grain size, sorting coefficient, skewness, and kurtosis (Fig. 2). Consistent with the lithology of core SO184-10043, grain size characteristics were described as follows:

The bottom section (280–382 cm) is predominantly characterized by silt (73.22%) with a lesser amount of sand (~ 12.63%) and clay (20.14%). The sand fraction increases towards the top of the section along with the mean grain size, with an average of 5.88 Φ, influenced by the composition of sand and clay. The sorting coefficient is an indicator of the degree of sorting in response to hydrodynamic conditions and averages 2.01. It shows no significant changes in the section, indicating relatively poor sorting. Skewness and kurtosis present similar trends and decrease upwards with insignificant fluctuations.

The middle section (105–280 cm) is the most variable. All of the parameters show noticeable changes. Silt fraction is predominant (64.62%), while sand fraction reaches its most representative value in this section (48.15%) at a depth of ~ 206 cm. The mean grain size also showed a similar trend with the silt, has an average value of 5.95 Φ, and is consistent with stronger bottom hydrodynamic conditions. The sorting coefficient varies from 1.70 to 2.21, reflecting various sedimentary environments. Skewness decreases upwards from – 0.78 to 1.62, indicating a complex sedimentary composition. Kurtosis reaches its highest value in this section (~ 2.82).

The upper section (0–105 cm) represents an opposite trend from the bottom section, where the average values of sand, silt, and clay fractions are determined to be 15.34%, 64.95%, and 19.72%, respectively. Silt remains the main fraction and reaches its lowest value at a depth of ~ 60 cm. Sand and clay fractions show a similar distribution trend in this section, being the most variable between 50 and 70 cm of depth. All of the grain-size parameters show substantial changes. The mean grain size gradually decreases upwards, with an average value of 5.8 Φ, and is consistent with stronger bottom hydrodynamic conditions. The sorting coefficient, skewness,

Fig. 2 Vertical distributions of grain size parameters of core SO184-10043; red dashed lines represent the boundary of three sections

and kurtosis start to vary from a depth of 105 cm to the top of the section.

Geochemistry

Major and trace element components are presented in Table 2. Among 10 major elements measured for the entire profile, SiO_2 is the dominant component, averaging 65.72%, followed by Al_2O_3 with an average of 14.33% and CaO with an average of 8.59%. These three elements amount to more than 85% of all the elements present. Other elemental proportions include 4.95% of TFe_2O_3, 3.50% of Na_2O, 1.66% of K_2O, 1.87% of MgO, 0.61% of TiO_2, 0.11% of P_2O_5, and 0.05% of MnO. Trace element concentration also fluctuates, ranging from 5.20×10^{-6} to 556.64×10^{-6} in the order of Ba > Sr > Zr > V > Pb > Zn > Cu > Cr > Ni > Co.

Throughout the length of the core, most elements display similar or reciprocal distribution patterns (Fig. 3). Three horizons (0–12.0 cm, 200–222 cm, and 350–370 cm) serve as important boundaries, where the elemental composition changes. As such, SiO_2, MnO, Na_2O, P_2O_5, and Zr reach relatively high values at these horizons, whereas Al_2O_3, MgO, Ba, Cr, Co, and Ni are characterized by the lowest content. Other portions of the core demonstrate little compositional changes.

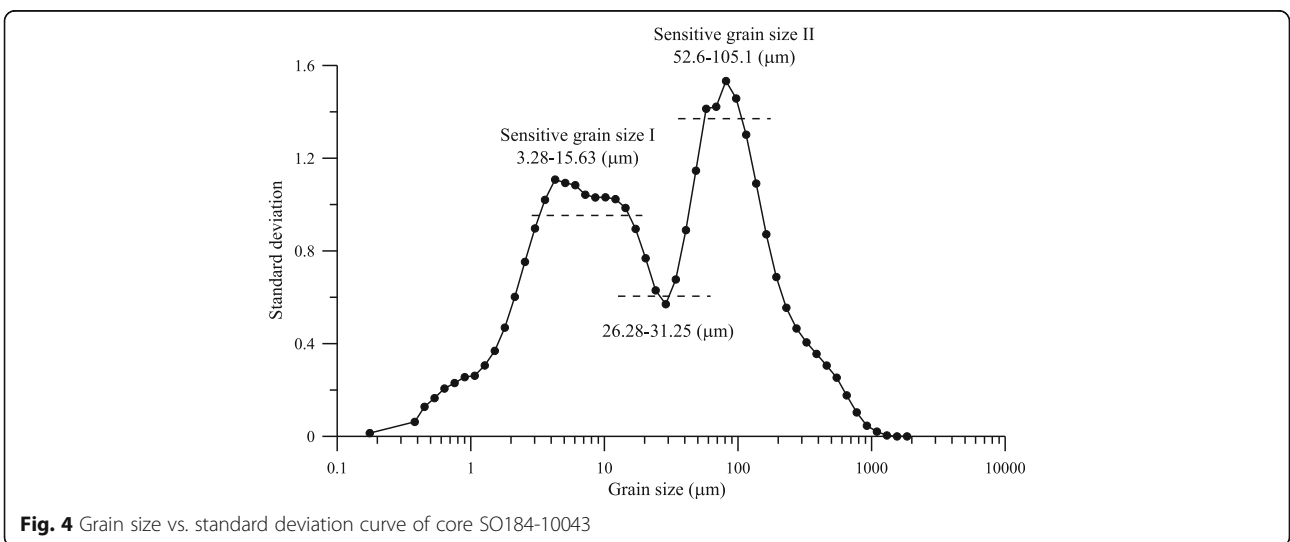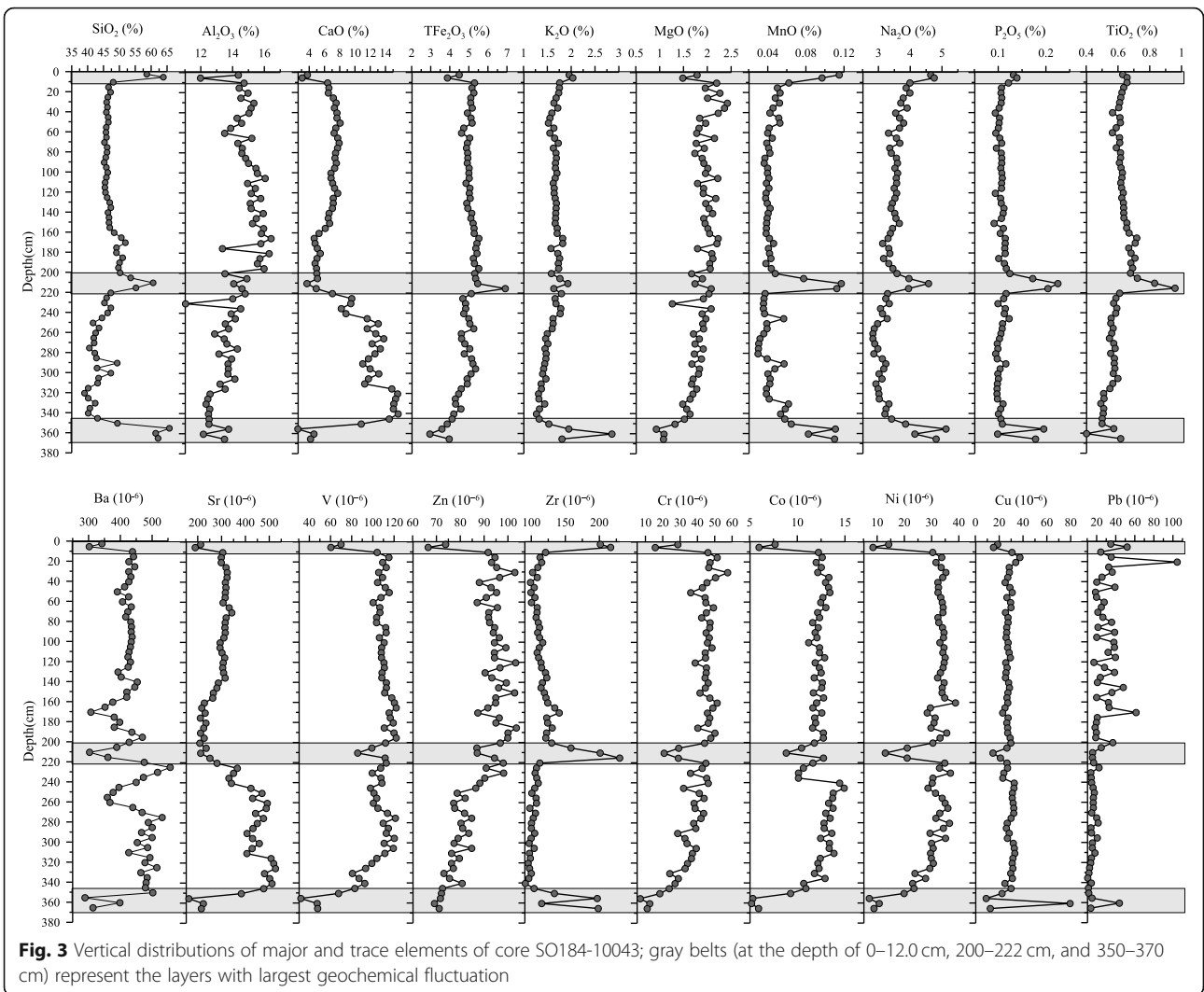## Discussion

Hydrodynamic condition

Sediment grain size is widely used to reconstruct past sedimentary environments and paleoclimate evolution. It also serves as a direct proxy of hydrodynamic conditions (Xiao et al. 2006; Cao et al. 2015). However, the transportation of marine sediments depends on a multitude of factors, which result in selective transportation and variable sediment compositions under different hydrodynamic conditions (Xiao et al. 2005; Liu et al. 2010). As marine sediments usually form mixtures of sediments in complex sedimentary environments and their constituent components can be delivered from different provenances, meaningful fraction selection from the bulk grain-size distribution is required to infer their significance for specific depositional conditions. In recent years, several mathematical and statistical methods have been developed, such as the Weibull function (Sun et al. 2002), end-member modeling of grain-size distributions (Stuut et al., 2002a, b; Prins et al. 2007), and analysis of grain-size populations with environmentally sensitive terrigenous components (Boulay et al. 2002; Sun et al. 2003). All these methods have been widely used to extract typical fractions to reveal a hydrodynamic evolution in the marginal sea settings. Herein, we applied a mathematical method "grain size vs. standard deviation" to extract the environmentally sensitive components, which reflect the variability in grain size in a sample group using each grain-size class. High standard deviation values tend to indicate high-frequency variability in grain-size classes in a sample group and vice versa. We used a standard deviation vs. grain-size class plot to identify the number of grain-size components and size range of each grain-size component in a sample group, where the components are closely related to the sedimentary environment (Stuut et al., 2002a, b; Xiang et al. 2006). We calculated the standard deviation of each grain-size grade using the terrigenous components in 74 samples of core SO184-10043 and defined two components sensitive to the sedimentary environment: 3.28–15.63 μm and 52.6–105.1 μm, with the boundary at 26.28–31.25 μm (Fig. 4).

Previous studies have shown that two sensitive components in a sedimentary environment are characteristics of continental margins and adjacent coastal areas controlled by normal hydrodynamic conditions (e.g., coastal currents, warm currents) and unstable hydrodynamic conditions (e.g., storm currents, earthquakes, waves) (Xiao et al. 2005; Xiang et al. 2006). Each of the two grain-size classes represents a population of grains with the highest variability through time (Xiao et al. 2006), while the boundary of these two populations is

Table 2 Composition of major and trace elements of sediment from core SO184-10043

Major element	Maximum value (%)	Minimum value (%)	Average value (%)	Trace element	Maximum value (10^{-6})	Minimum value (10^{-6})	Average value (10^{-6})
SiO_2	65.72	39.00	47.30	Ba	556.64	288.63	430.48
Al_2O_3	16.42	11.04	14.33	Cr	57.42	7.01	39.78
CaO	15.66	2.50	8.59	Sr	525.90	162.54	338.00
TFe_2O_3	6.91	2.96	4.95	V	122.00	32.00	104.30
K_2O	2.85	1.27	1.66	Zn	103.51	69.15	88.67
MgO	2.42	0.93	1.87	Zr	229.79	91.13	119.24
MnO	0.12	0.03	0.05	Co	14.91	5.20	12.03
Na_2O	5.12	2.82	3.50	Ni	38.75	7.11	30.62
P_2O_5	0.23	0.09	0.11	Cu	79.46	9.04	28.27
TiO_2	0.96	0.40	0.61	Pb	104.43	10.55	24.45

Fig. 3 Vertical distributions of major and trace elements of core SO184-10043; gray belts (at the depth of 0–12.0 cm, 200–222 cm, and 350–370 cm) represent the layers with largest geochemical fluctuation

**Fig. 4** Grain size vs. standard deviation curve of core SO184-10043

characterized by the lowest standard deviation value and implies negligible changes within this proportion of the grain-size population in the siliciclastic fraction. Hence, we can infer that these two grain-size populations of core SO184-10043 were mainly controlled by coastal currents driven by monsoon systems and by wave currents driven by storms or tsunami. Considering that the northwest (Indonesian) monsoon current is stronger than the southeast Malaysian-Australian monsoon current (Fig. 1), we suggest that the finer population (sensitive component I 3.28–15.63 μm) was mainly transported by the stronger Indonesian monsoon current. A large-amplitude fluctuation of the mean grain size and content further confirms its response being sensitive to sedimentary variation (Fig. 5). The coarser grain-size population (sensitive component II 52.6–105.1 μm) shows a slight temporal change that might reflect a stronger current. Regardless, as fraction II appears continuously in the core, its origin may be related to normal sedimentation driven by a local wave system. Consequently, sensitive component I is chosen to reflect the evolution of the hydrodynamic conditions in this study. As shown in Fig. 5, we were able to distinguish between the glacial-interglacial responses of hydrodynamic intensity within the study area. During the late marine isotope stage (MIS) 3 and Holocene, a higher mean grain size of sensitive component I is interpreted to reflect a stronger monsoon current, probably associated with a stronger northwest monsoon reconstructed by paired SST and $\delta^{18}O_{sw}$ (Govil and Naidu 2011). Limited by the quantity and resolution of the analyzed data, we obtained less detailed core information for MIS 3. However, the resolution for the Holocene portion of the core was not compromised. The mean

grain size of sensitive component I changed from 8 to 8.8 μm, revealing incremental hydrodynamic conditions coherent with the record from the Andaman Sea and the Bay of Bengal (Cao et al. 2015; Li et al. 2019), where larger sediment fractions could be transported from the adjacent continent to the sea. On the contrary, the mean grain-size value of sensitive component I was lower during the last glaciation-deglaciation phase, revealing weak hydrodynamic conditions, controlled by weaker monsoon systems (Mohtadi et al. 2014; Gebregiorgis et al. 2016). The lowest value of sensitive component I was observed at 15 ka BP and coincided with the weakest monsoon record in the northeastern Indian Ocean (Rashid et al. 2007; Govil and Naidu 2011). On a millennial time scale, a number of significant grain-size fluctuations were identified by examining a sensitive grain-size curve, such as the Heinrich Stadial 1 (HS1), B/A, and Younger Dryas (YD) deglaciation events, which corresponded to larger climate and environmental changes (Li et al. 2016).

Chemical weathering intensity

Elemental geochemistry composition is related to sediment source, grain size, and dynamic conditions, which are essential to reveal a sedimentary environment and climate intensity in the past epochs (Tao et al. 2006). Climatic and environmental changes contribute to the concentration, transportation, and deposition of certain elements (Young and Nesbitt 2001). Thus, the content and assemblage of specific elements may be a good indicator of the past climates and depositional environments (Liu et al. 2010), especially for the weathering and paleoclimatic processes recorded in sediments (Yan et al.

Fig. 5 Content and mean grain size of two sensitive components from core SO184-10043
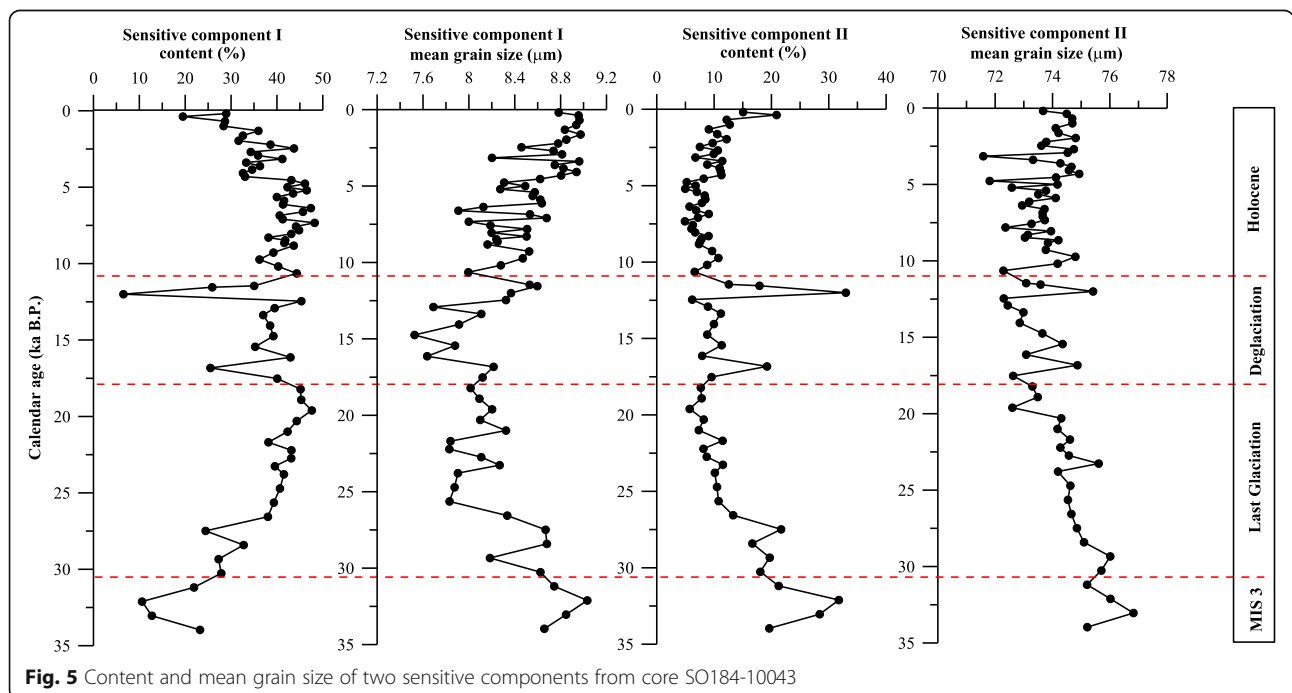
2002; Tao et al. 2006; Zhao et al. 2008; Liu et al. 2011). Chemical weathering appears to drive relatively mobile elements, such as Na, Ca, and Sr, to migrate in their aqueous form (Tao et al. 2006), while conservative elements, such as Ti and Al, remain stable in the sediments (Yang et al. 2006). The differential mobility allows us to use the ratios of these elements in order to infer past climatic conditions. The following ratios of elements are the most commonly used in the vicinity of the Asian marginal seas: Al_2O_3/Na_2O, K_2O/Na_2O, CaO/K_2O, CaO/MgO, CaO/Sr, and Rb/Sr (Young and Nesbitt 2001; Tao et al. 2006; Ye et al. 2010; Liu et al. 2011). In addition, the Chemical Index of Alteration (CIA = $[Al_2O_3/(Al_2O_3 + CaO^* + Na_2O + K_2O)] \times 100$) (Nesbitt et al. 1980; Nesbitt and Young 1989, 1996; Delaney et al. 1993; Nyakairu and Koeberl 2000; Young and Nesbitt 2001; Yan et al. 2002) is frequently used to estimate the intensity of weathering (Yang et al. 2004), where CaO^* is CaO in a silicate fraction calculated by the Honda and Shimizu's formula: $[CaO^* = 0.35 \times 2(Na_2O\%)/62]$ (Nesbitt and Young 1982).

The Sumatra offshore waters are situated within the seasonal features of the following monsoon systems: the southeast Malaysian-Australian monsoon and northwest Indonesian monsoon. These monsoon systems determine Sumatra's regional precipitation and temperature patterns. In this study, we utilized the CIA, CaO/MgO, and Ba/Sr proxies for the reconstruction of chemical weathering intensity to deduce the monsoon evolution process further. These geochemical proxies are regarded as synchronous with changes in the oxygen isotope stages since the last glacial period, reflecting rapid sediment deposition and the influence of climate (Fig. 6).

Four phases were identified from the core bottom to top as follows: MIS 3, last glaciation, deglaciation, and the Holocene. The geochemical proxies during MIS 3 and the Holocene showed similar features, with higher ratios of CIA and Ba/Sr and lower ratios of CaO/MgO, indicating increased weathering and erosion rates in the source areas, dominated by a warm and humid climate during these periods. Higher precipitation and temperatures tend to be accompanied by active chemical weathering (Yang and Li 1999). Our results are supported by the $\delta^{18}O$ values of planktonic foraminifera and SST reconstruction in the Andaman Sea (Rashid et al. 2007), where intense precipitation and high temperatures were reported for MIS 3 and the Holocene (Marzin et al. 2013). Such climatic conditions caused higher river runoff, reflected in a high Ba/Ca ratio from the planktonic foraminifera *G. sacculifer* shells (Gebregiorgis et al. 2016; Sijinkumar et al. 2016). On the contrary, lower CIA and Ba/Sr values and higher CaO/MgO ratios during the last glaciation-deglaciation indicate weaker chemical weathering intensity, controlled by low precipitation and decreased temperatures. The reduced chemical weathering and erosion rates were also reported from the Andaman Sea during MIS 2 (Colin et al. 1998; Miriyala et al. 2017). Similar to the sensitive grain-size proxy, the decreasing CaO/MgO, and increasing CIA, Ba/Sr during the deglaciation period also changed sharply, revealing a warm and moist climate generated after the last glaciation. Some minor variations in the chemistry proxies were identified from the following intervals: 12.5–12, 17–15, and 34–32 ka BP. These variations imply the instability of chemical weathering intensity on a millennial time scale. Similar trends were found for the sea surface
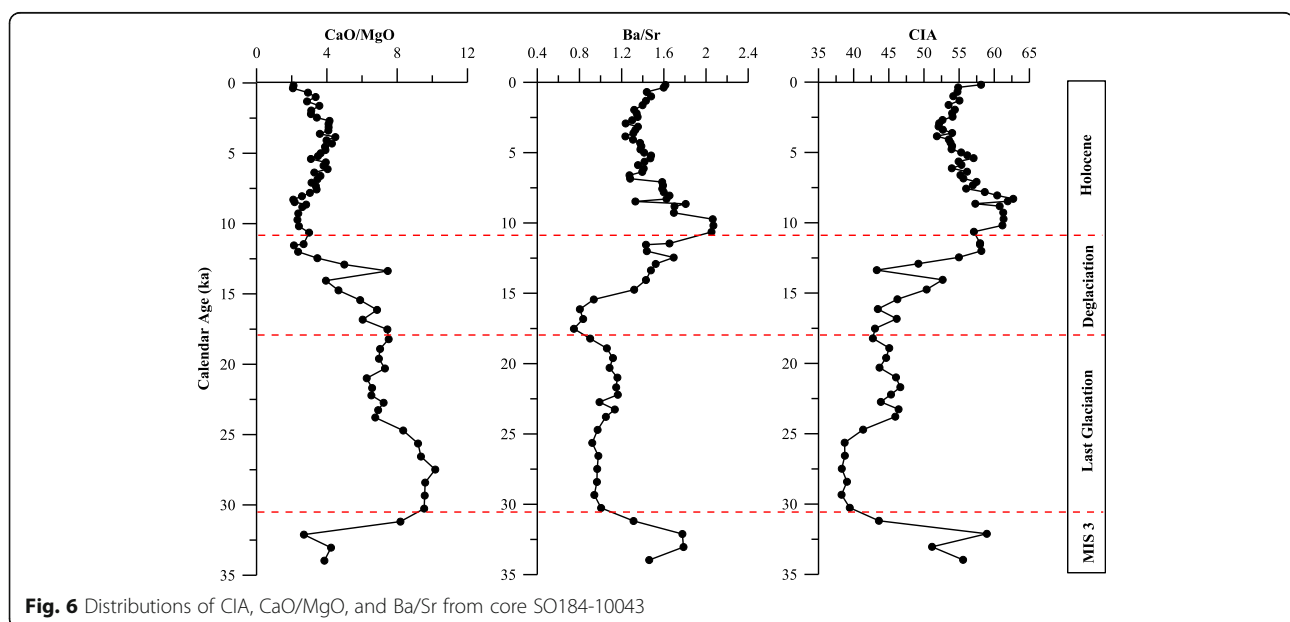
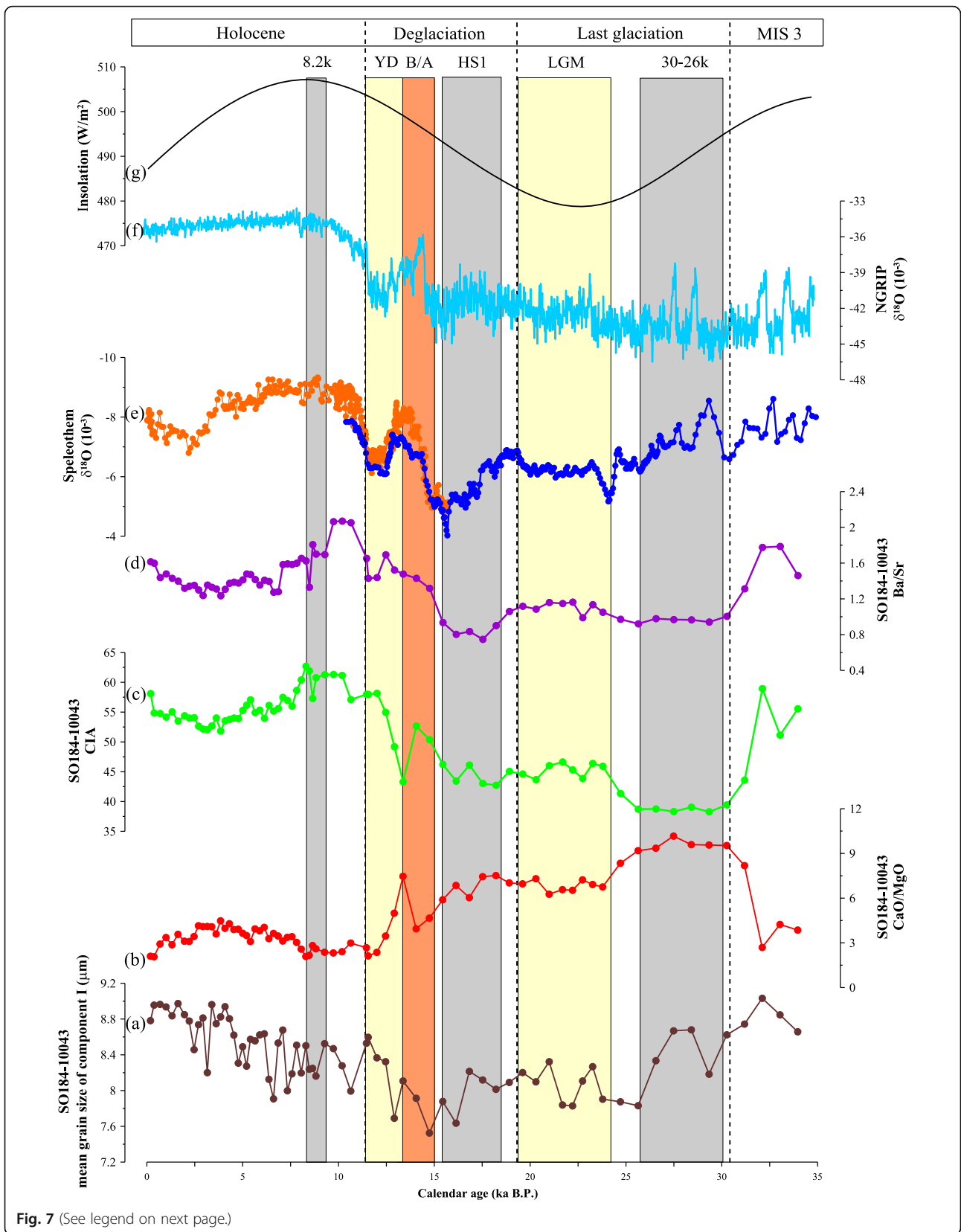Fig. 6 Distributions of CIA, CaO/MgO, and Ba/Sr from core SO184-10043

Fig. 7 (See legend on next page.)

(See figure on previous page.)
Fig. 7 Paleoclimatic proxies and referenced data plotted as a function of age (ka B.P.): (a) mean grain size of sensitive component I from core SO184-10043 (this study); (b) CaO/MgO from core SO184-10043 (this study); (c) CIA from core SO184-10043 (this study); (d) Ba/Sr from core SO184-10043 (this study); (e) records of speleothem $\delta^{18}O$ from Dongge Cave in the southern China (Yuan et al. 2004) and Hulu Cave in the eastern China (Wang et al. 2001); (f) records of ice core (NGRIP) $\delta^{18}O$ from Greenland (Andersen et al. 2006; Rasmussen et al. 2006); (g) integrated summer insolation variations at 30° N over June, July, and August (Berger 1978). Grey, yellow, and orange bars in this figure represent global cold events recorded in our core SO184-10043

temperature and seawater salinity proxies (Mohtadi et al. 2014; Li et al. 2016).

Paleoclimate reconstruction for the past 35 kyr

Monsoonal climate dominates over the northern Indian Ocean. Its close relationship with global climate changes during the late Pleistocene was revealed by marine sedimentary records (Schulz et al. 1998, Mohtadi et al., 2014). The results of our study show that both monsoon current and chemical weathering coincide with the glacial-interglacial changes in the Northern Hemisphere. During the late MIS 3 and Holocene, higher values of sensitive grain size, increased CIA, and Ba/Sr ratios, as well as lower CaO/MgO ratios, reflect a stronger monsoon current and heightened chemical weathering intensity, which were likely connected to a stronger northwest monsoon that carried warm and moist air from the Asian continent to Indonesia. Evidence from land precipitation (Wang et al. 2001), seawater salinity (Li et al. 2016), sea surface temperature (Mohtadi et al. 2014), and paleoproductivity (Xu et al. 2017) supports the suggested stronger northwest monsoon. High temperature and increased precipitation were able to accelerate weathering, erosion, and the terrestrial influx into the sea from the surrounding territories, whereas a monsoon current was characterized by higher energy that transported coarser sediments to the continental shelf. During the last glaciation-deglaciation phase, lower sensitive grain size, decreased CIA, and Ba/Sr ratios, as well as higher CaO/MgO ratios, reveal a weaker monsoon current and diminished chemical weathering intensity, which were likely controlled by a weaker monsoon system. Low precipitation and decreased temperatures during MIS 2 reduced the transport of the chemical weathering and erosion products to the core location. We also identified other processes for this period. For instance, the monsoon system was at its weakest point during the last glaciation, while a strong rebound occurred from 16 to 11 ka BP. Seawater $\delta^{18}O$ was measured from the nearby cores, SO189-119KL and SO189-39KL, and presented significantly decreased values (Mohtadi et al. 2014), which coincides with increased summer insolation in the Northern Hemisphere (Li et al. 2016).

The movement of rainfall belt in a monsoon area is controlled by the displacement of the ITCZ, which, in turn, is principally driven by orbital changes in solar insolation (Fleitmann et al. 2007; Goodbred 2003; Philander et al.

1996; Wang et al. 2005; Xie and Saito 2001). The almost synchronous changes in the indices of sensitive component I and chemical weathering seem to be modulated by the orbital-scale variations in 30° N July insolation, suggesting a prominent response to the Northern Hemisphere climate changes (Fig. 7). The highest CIA and Ba/Sr ratios and the lowest CaO/MgO values were noted for 10–8 ka BP. The highest insolation values appeared between 12 and 11 ka BP. The opposite trend was observed when insolation reached its minimum at 25 ka BP (Berger and Loutre 1991; Laskar et al. 2004). Therefore, we infer that orbital-scale changes in insolation influenced the glacial-interglacial paleoclimate changes over the past 35 kyr in the southernmost Sumatra waters.

On a millennial timescale, cold events occurred during the following intervals: HS1 (18–15 ka BP), Last Glacial Maximum (LGM; 23–18 ka BP), YD (11–10 ka BP), and 8.2 ka BP. The same events were identified in core SO184-10043, indicating their co-occurrence with the Northern Hemisphere cold events. Hydrodynamic conditions and chemical weathering intensity were weak during these events, which were observed in ice core records from the northern Atlantic (Andersen et al. 2006; Rasmussen et al. 2006). It should be pointed out that abnormal weakening of hydrodynamic conditions and chemical weathering from 30 to 26 ka BP was recorded in our core sediments. This period coincides with a reduced-precipitation event in the Indian Ocean (Ali et al. 2015; Sijinkumar et al. 2016), revealing the predominant role of monsoon systems in the sedimentary processes.

We used a power spectrum analysis (PSA) to investigate the periodicity of climate records and its possible driving forces in core SO184-10043. The CIA and MgO/CaO time series were analyzed using REDFIT35 (Schulz and Mudelsee 2002), which have been shown to have a high performance in PSA for unevenly spaced time series. PSA of the CIA and MgO/CaO time series showed maximum power at periodicities centered at 3.0–3.1 ka, 2.2–2.3 ka, and ~ 1.0 ka, all of which are characteristic of solar activity (Stuiver et al. 1995; Wang et al. 2005) (Fig. 8). Though the interpretation of our results is ultimately limited by the marine sediment core resolution and age uncertainty of the AMS[14]C dating, our results suggest a possible influence of changes in solar activity on the Sumatra maritime climate on multi-decadal and multi-centennial scales (Hong et al. 2001; Xiao et al. 2006). These data further support the
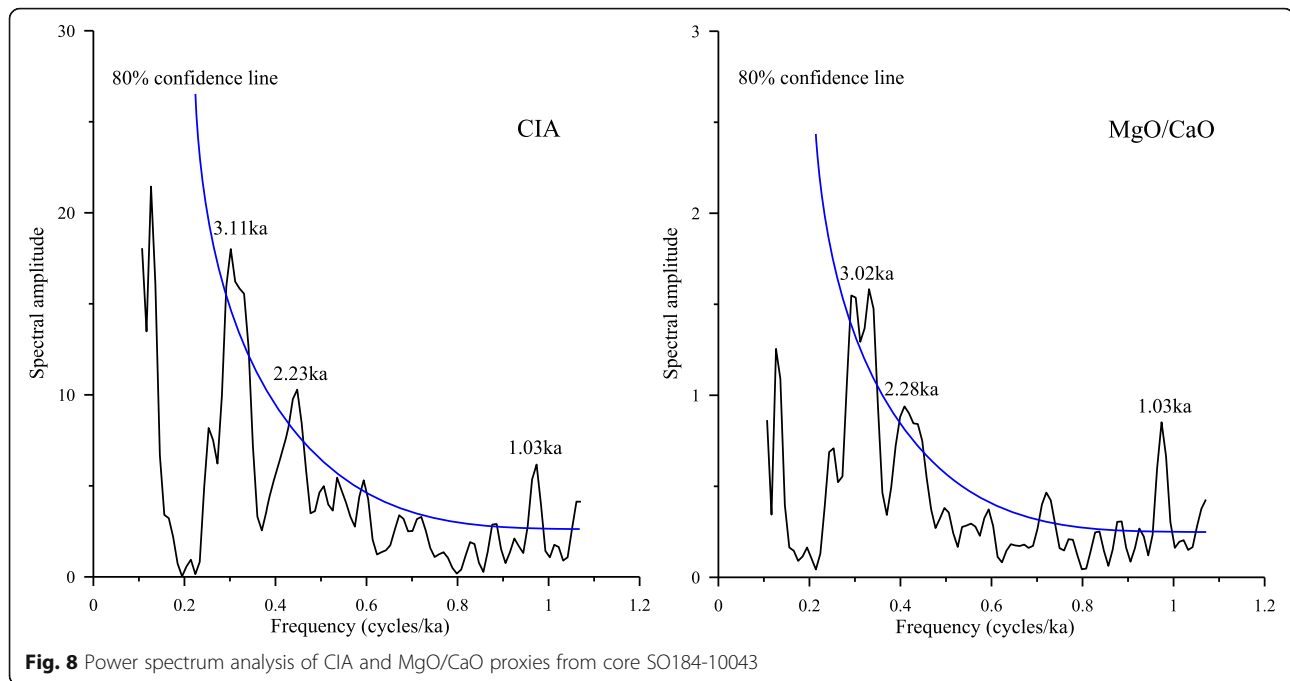
Fig. 8 Power spectrum analysis of CIA and MgO/CaO proxies from core SO184-10043

monsoon evolution in the tropical Indian Ocean during the Late Pleistocene and its dependence on the Northern Hemisphere climate changes.

Conclusions

We conducted a paleoclimatic reconstruction for core SO184-10043 collected from the southernmost coast of Sumatra using sedimentological, geochemical, and elemental proxies in order to reconstruct the monsoon evolution and its response to the Northern Hemisphere climate changes.

On a glacial-interglacial timescale, both monsoon current and chemical weathering coincided with summer insolation in the Northern Hemisphere and showed a clear response to the glacial-interglacial changes. Higher values of sensitive grain size, CIA, and Ba/Sr, as well as lower CaO/MgO ratios, indicated a stronger monsoon current and chemical weathering intensity in the late MIS 3 and Holocene. Such climate conditions were likely controlled by a stronger northwest monsoon that carried warm and moist air from the Asian continent to Indonesia. Lower sensitive grain size, CIA, and Ba/Sr ratio with higher CaO/MgO values revealed a weaker monsoon current and diminished chemical weathering intensity during the last glaciation-deglaciation phase, which was predominantly controlled by a weaker monsoon system.

On a millennial timescale, in core SO184-10043, we were able to identify a number of global cold events, such as the one at 30–26 ka BP, HS1 (18–15 ka BP), LGM (23–18 ka BP), YD (11–10 ka BP), and 8.2 ka BP,

which occurred simultaneously with the Northern Hemisphere cold events. We also applied PS and identified periodicities of ~ 7.9 ka, 3.0–3.1 ka, 2.2–2.3 ka, and ~ 1.0 ka in our core records. We related these periodicities to solar-induced climate changes, which further support our findings of the monsoon evolution in the tropical Indian Ocean in the late Pleistocene and its co-incidence with the Northern Hemisphere climate changes.

Supplementary information

Authors' contributions

SFL participated in the data analysis and research idea design and completed the main work of the paper. HZ participated in the analysis of the elements and drafted the manuscript. XFS conceived of the study and

Author details
[1]Key Laboratory of Marine Geology and Metallogeny, First Institute of Oceanography, Ministry of Natural Resources, Qingdao 266061, China. [2]Laboratory for Marine Geology, Qingdao National Laboratory for Marine Science and Technology, Qingdao 266061, China. [3]Institute of Earth Sciences, Taiwan Ocean University, Keelung 20224, Taiwan. [4]College of Marine Geosciences, Ocean University of China, Qingdao 266100, China. [5]Marine Research Center, Agency of Research and Human Resources for Marine and Fisheries, Ministry of Marine Affairs and Fisheries, Jakarta 14430, Indonesia. [6]Center for Geological Survey, Geological Agency, Ministry of Energy and Mineral Resources, Bandung 40122, Indonesia. [7]Research Center for Geotechnology, Indonesia Institute of Sciences, Bandung 40135, Indonesia. [8]Graduate program in Earth Sciences, Faculty of Earth Sciences and Technology, Institute of Technology Bandung, Bandung 40132, Indonesia.

References
Ali S, Hathorne EC, Frank M, Gebregiorgis D, Stattegger K, Stumpf R, Kutterolf S, Johnson JE, Giosan L (2015) South Asian monsoon history over the past 60 kyr recorded by radiogenic isotopes and clay mineral assemblages in the Andaman Sea. Geochemistry Geophysics Geosystems 16(2):505–521

Andersen KK, Svensson A, Johnsen SJ, Rasmussen SO, Bigler M, Röthlisberger R, Ruth U, Siggaard-Andersen M-L, Steffensen JP, Dahl-Jensen D, Vinther BM, Clausen HB (2006) The Greenland ice core chronology 2005, 15-42 ka. Part 1: constructing the time scale. Quat Sci Rev 25:3246–3257

Berger AL (1978) Long-term variations of daily insolation and quaternary climatic changes. J Atmos Sci 35(12):2362–2367

Berger AL, Loutre MF (1991) Insolation values for last 10 million years. Quat Sci Rev 10(4):297–317

Boulay S, Colin C, Trentesaux A, Pluquet F, Bertaux J, Blamart D, Buehring C, Wang P (2002) Mineralogy and sedimentology of Pleistocene sediments on the South China Sea (ODP site 1144). In: Prell, W.L., Wang, P., Blum, P., Rea, D. K., Clemens, S.C. (Eds), proceeding of the ocean drilling program scientific results 184, 1-21.

Cao P, Shi XF, Li WR, Liu SF, Yao ZQ, Hu LM, Somkiat K, Narumol K (2015) Sedimentary responses to the Indian summer monsoon variations recorded in the southeastern Andaman Sea slope since 26 ka. J Asian Earth Sci 114: 512–525

Clemens S, Prell WL, Murray D, Shimmield G, Weedon G (1991) Forcing mechanisms of the Indian Ocean monsoon. Nature 353:720–725

Colin C, Kissel C, Blamart D, Turpin L (1998) Magnetic properties of sediments in the bay of Bengal and the Andaman Sea: implication of rapid North Atlantic Ocean climatic events on the strength of the Indian monsoon. Earth Planet Sci Lett 160:623–635

Colin C, Turpin L, Bertaux J, Desprairies A, Kissel C (1999) Erosional history of the Himalayan and Burman ranges during the last two glacial-interglacial cycles. Earth Planetary Science Letters 171:647–660

Cullen JL (1981) Microfossil evidence for changing salinity patterns in the bay of Bengal over the last 20,000 years. Palaeogeogr Palaeoclimatol Palaeoecol 35: 315–356

Dahl KA, Oppo DW (2006) Sea surface temperature pattern reconstructions in the Arabian Sea. Paleoceanography 21, PA 1014.

Delaney ML, Linn LJ, Druffel RM (1993) Seasonal cycles of manganese and cadmium in coral from the Galapagos Islands. Geochim Cosmochim Acta 57: 347–354

Fleitmann D, Burns SJ, Mangini A, Mudelsee M, Kramers J, Villa I, Neff U, Al-Subbary AA, Buettner A, Hippler D, Matter A (2007) Holocene ITCZ and Indian monsoon dynamics recorded in stalagmites from Oman and Yemen (Socotra). Quat Sci Rev 26:170–188

Gebregiorgis D, Hathorne EC, Sijinkumar AV, Nath BN, Nürnberg D, Frank M (2016) South Asian summer monsoon variability during the last ~54 kyrs inferred from surface water salinity and river run off proxies. Quat Sci Rev 138:6–15

Gingele FX, De Deckker P, Girault A, Guichard F (2002) History of the South Java current over the past 80 ka. Palaeogeogr Palaeoclimatol Palaeoecol 183(3-4): 247–260

Goodbred SL (2003) Response of the Ganges dispersal system to climate change: a source-to-sink view since the last interstade. Sediment Geol 162:83–104

Govil P, Naidu PD (2011) Variations of Indian monsoon precipitation during the last 32 kyr reflected in the surface hydrography of the Western Bay of Bengal. Quat Sci Rev 30:3871–3879

Hong YT, Wang ZG, Jiang HB, Lin QH, Hong B, Zhu YX, Wang Y, Xu LS, Leng XT, Li HD (2001) A 6000-year record of changes in drought and precipitation in northeastern China based on a $\delta^{13}C$ time series from peat cellulose. Earth Planet Sci Lett 185:111–119

Kroon D, Steens TNF, Troelstra SR (1991) Onset of monsoonal related upwelling in the western Arabian Sea as revealed by planktonic foraminifers. Proceedings of the Ocean Drilling Program 117:257–263

Laskar J, Robutel P, Joutel F, Gastineau M, Correia ACM, Levrarad B (2004) A long term numerical solution for the insolation quantities of earth. Astron Astrophys 428:261–285

Li J, Liu S, Shi X, Zhang H, Fang X, Cao P, Yang G, Xue X, Somkiat K, Narumol K (2019) Sedimentary responses to the sea level and Indian summer monsoon changes in the central bay of Bengal since 40 ka. Marine Gology 415:105947

Li Z, Shi X, Chen M-T, Wang H, Liu S, Xu J, Long H, Troa RA, Zuraida R, Triarso E (2016) Late Quaternary fingerprints of precession and sea level variation over the past 35 kyr as revealed by sea surface temperature and upwelling records from the Indian Ocean near southernmost Sumatra. Quat Int 425: 282–291

Liu S, Shi X, Fang X, Dou Y, Liu Y, Wang X (2014) Spatial and temporal distributions of clay minerals in mud deposits on the inner shelf of the East China Sea: implications for paleoenvironmental changes in the Holocene. Quat Int 349:270–279

Liu S, Shi X, Liu Y, Qiao S, Yang G, Fang X, Wu Y, Li C, Li X, Zhu A, Gao J (2010) Records of the east Asian winter monsoon from mud area in the inner shelf of the East China Sea since the mid-Holocene. Chin Sci Bull 55(21):2306–2314

Liu S, Shi X, Liu Y, Wu Y, Yang G (2011) Environmental record from the mud area on the inner continental shelf of the East China Sea since the mid-Holocene. Acta Oceanol Sin 30:43–52

Lückge A, Mohtadi M, Rühlemann C, Scheeder G, Vink A, Reinhardt L, Wiedicke M (2009) Monsoon versus ocean circulation controls on paleoenvironmental conditions off southern Sumatra during the past 300,000 years. Paleoceanography 24:PA1208

Marzin C, Kallel N, Kageyama M, Duplessy JC (2013) Glacial fluctuations of the Indian monsoon and their relationship with North Atlantic climate: new data and modelling experiments. Clim Past 9(5):2135–2151

Miriyala P, Sukumaran NP, Nath BN, Ramamurty PB, Sijinkumar AV, Vijayagopal B, Ramaswamy V, Sebastian T (2017) Increased chemical weathering during the deglacial to mid-Holocene summer monsoon intensification. Sci Rep 7:1–11

Mohtadi M, Prange M, Oppo DW, De PR, Merkel U, Zhang X, Steinke S, Lückge A (2014) North Atlantic forcing of tropical Indian Ocean climate. Nature 509(7498):76–80

Murgese DS, De Deckker P, Spooner MI et al (2008) A 35000 year record of changes in the eastern Indian Ocean offshore Sumatra. Palaeogeogr Palaeoclimatol Palaeoecol 265:195–213

Nesbitt HW, Markovics G, Price RC (1980) Chemical processes affecting alkalis and alkaline earths during continental weathering. Geochim Cosmochim Acta 44: 1659–1666

Nesbitt HW, Young GM (1982) Early proterozoic climates and plate motions inferred from major element chemistry of lutites. Nature 299:715–717

Nesbitt HW, Young GM (1989) Formation and diagenesis of weathering profiles. J Geology 97(2):129–147

Nesbitt HW, Young GM (1996) Petrogenesis of sediments in the absence of chemical weathering: effects of abrasion and sorting on bulk composition and mineralogy. Sedimentology 43:341–358

Nyakairu GWA, Koeberl C (2000) Mineralogical and chemical composition and distribution of rare earth elements in clay-rich sediments from Central Uganda. Geochem J 35:13–28

Philander SGH, Gu D, Lambert G, Li T, Halpern D, Lau NC, Pacanowski RC (1996) Why the ITCZ is mostly north of the equator. J Clim 9(12):2958–2972

Prell WL, Curry WB (1981) Faunal and isotopic indices of monsoonal upwelling: Western Arabian Sea. Oceanol Acta 4:91–98

Prell WL, Murray WW, Clemens SC, Anderson DM (1992) Evolution and variability of the Indian Ocean summer monsoon: evidence from western Arabian Sea drilling program. Synthesis of results from scientific drilling in the Indian Ocean 70:447–469

Prins MA, Vriend M, Nugteren G, Vandenberghe J, Lu H, Zheng H, Weltje GJ (2007) Late Quaternary aeolian dust input variability on the Chinese loess plateau: inferences from unmixing of loess grain-size records. Quat Sci Rev 26:230–242

Qin Y, Zhao Y, Chen L, Chen S (1987) Geology of the East China Sea (in Chinese). Science Press, Beijing, pp 1–286

Qu T, Du Y, Strachan J, Meyers G, Slingo JM (2005) Sea surface temperature and its variability in the Indonesian region. Oceanography 18(4):50–61

Rashid H, Flower BP, Poore RZ, Quinn TM (2007) A ~25 ka Indian Ocean monsoon variability record from the Andaman Sea. Quat Sci Rev 26:2586–2597

Rasmussen SO, Andersen KK, Svensson AM, Steffensen JP, Vinther BM, Clausen HB, Siggaard-Andersen ML, Johnsen SJ, Larsen LB, Dahl-Jensen D, Bigler M, Röthlisberger R, Fischer H, Goto-Azuma K, Hansson ME, Ruth U (2006) A new Greenland ice core chronology for the last glacial termination. J Geophys Res 111:D06102

Reimer PJ, Bard E, Bayliss A, Beck JW, Blackwell PG, Ramsey CB, Buck CE, Cheng H, Edwards RL, Friedrich M, Grootes PM, Guilderson TP, Haflidason H, Hajdas I, Hatté C, Heaton TJ, Hoffmann DL, Hogg AG, Hughen HA, Kaiser KF, Kromer B, Manning SW, Niu M, Reimer RW, Richards DA, Scott EM, Southon JR, Staff RA, Turney CSM, Plicht J (2013) Intcal 13 and marine 13 radiocarbon age calibration curves 0-50,000 years cal BP. Radiocarbon 55(4):1869–1887

Schulz H, Rad U, Erlenkeuser H (1998) Correlation between Arabian Sea and Greenland climate oscillations of the past 110,000 years. Nature 393:54–57

Schulz M, Mudelsee M (2002) REDFIT: estimating red-noise spectra directly from unevenly spaced paleoclimatic time series. Comput Geosci 28:421–426

Sijinkumar AV, Clemens S, Nath BN, Prell W, Benshila R, Lengaigne M (2016) δ^{18}O and salinity variability from the last glacial maximum to recent in the bay of Bengal and Andaman Sea. Quat Sci Rev 135:79–91

Sijinkumar AV, Nath NB, Possnert G (2011) Pulleniatina minimum events in the Andaman Sea (NE Indian Ocean)-implications for winter monsoon and thermocline changes. Mar Micropaleontol 81:88–94

Southon J, Kashgarian M, Fontugne M, Metivier B, Yim WW-S (2002) Marine reservoir corrections for the Indian Ocean and Southeast Asia. Radiocarbon 44:167–180

Spooner MI, Barrows TT, De Deckker P, Paterne M (2005) Palaeoceanography of the Banda Sea, and late Pleistocene initiation of the northwest monsoon. Glob Planet Chang 49(1-2):28–46

Stuiver M, Grootes PM, Braziunas TF (1995) The GISP2 δ^{18}O climate record of the past 16,500 years and the role of the sun, ocean and volcanoes. Quat Res 44:341–354

Stuut JBW, Prins MA, Ralph RS, Weltje GJ, Jansen JH (2002a) A 300-kyr record of aridity and wind strength in southwestern Africa: inferences from grain-size distributions of sediments on Walvis ridge, SE Atlantic. Mar Geol 180:221–233

Stuut JBW, Prins MA, Schneider RR, Weltje GJ, Jansen JHF, Postma G (2002b) A 300-kyr record of aridity and wind strength in southwestern Africa: inferences from grain-size distributions of sediments on Walvis ridge SE Atlantic. Mar Geol 180:221–233

Sun D, Bloemendal J, Rea DK, Jiang F, An Z (2002) Grain-size distribution function of polymodal sediments in hydraulic and aeolian environments, and numerical partitioning of the sedimentary components. Sediment Geol 152(40606):263–277

Sun Y, Gao S, Li J (2003) Primary analysis on the sensitive grain size of terrigenous sediment to environments in marginal sea (in Chinese with English abstract). Chin Sci Bull 48:83–86

Tao J, Chen M, Xu S (2006) A Holocene environmental record from the southern Yangtze River delta, eastern China. Palaeogeogr Palaeoclimatol Palaeoecol 230:204–229

Tomczak M, Godfrey JS (2001) Regional oceanography: an introduction [electro-Nic]. Daya, Delhi, India, pp 1–391

Wang P, Clemens S, Beaufort L, Braconnot P, Ganssen G, Jian Z, Kershaw P, Sarnthein M (2005) Evolution and variability of the Asian monsoon system: state of the art and outstanding issues. Quat Sci Rev 24:595–629

Wang Y, Cheng H, Edwards RL, An Z, Wu J, Shen C, Dorale JA (2001) A high-resolution absolute-dated late Pleistocene monsoon record from Hulu cave, China. Science 294:2345–2348

Wijffels SE, Hautala S, Bray H, Meyers G (1996) The WOCE Indonesian throughflow repeat hydrography sections: I10 and IR6. International WOCE Newsletter 24:25–28

Wyrtki K (1961) Scientific results of marine investigations of the South China Sea and the Gulf of Thailand. In: NAGA report 2. University of California, Scripps Institute of Oceanography, La Jolla, CA

Wyrtki K (1962) The upwelling in the region between Java and Australia during the southeast monsoon, Aust. Mar Freshw Res 13:217–225

Xiang R, Yang ZS, Satio Y, Guo Z, Fan D, Li Y, Xiao S, Shi X, Chen M (2006) East Asia winter monsoon changes inferred from environmentally sensitive grain-size component records during the last 2300 years in mud area southwest off Cheju Island, ECS. Sci China Ser D Earth Sci 49:604–614

Xiao S, Li A, Liu J, Chen M, Xie Q, Jiang F, Li T, Xiang R, Chen Z (2006) Coherence between solar activity and the East China Asian winter monsoon variability in the past 8000 years from Yangtze River-derived mud in the East China Sea. Palaeogeograpphy, Palaeoclimatology, Palaeoecology 237:293–304

Xie S, Saito K (2001) Formation and variability of a northerly ITCZ in a hybrid coupled AGCM: continental forcing and oceanic-atmospheric feedback. J Clim 14:1262–1276

Xu Y, Wang L, Yin X, Ye X, Li D, Liu S, Shi X, Troa RA, Zuraida R, Triarso E, Hendrizan M (2017) The influence of the Sunda Strait opening on paleoenvironmental changes in the eastern Indian Ocean. J Asian Earth Sci 146:402–411

Yan W, Gu S, Chen Z, Chen M (2002) Characteristics of major elements of sediments in core 97-37 from southern South China Sea and potential implications to paleoenvironment (in Chinese with English abstract). Journal of Tropical Oceanography 21:75–83

Yang S, Ding F, Ding Z (2006) Pleistocene chemical weathering history of Asian arid and semi-arid regions recorded in loess deposits of China and Tajikistan. Geochimica 70:1695–1709

Yang S, Li C (1999) Characteristic element compositions of the Yangtze and the Yellow River sediments and their geological background (in Chinese with English abstract). Mar Geol Quat Geol 19(2):19–26

Yang S, Li C, Yang D, Li X (2004) Chemical weathering of the loess deposits in the lower Changjiang Valley, China, and paleoclimatic implications. Quat Int 117:27–34

Ye H, Zhang K, Chen F, Chen R, Xu Y, Ji J (2010) The response of the main and trace element concentrations to climate evolument in 8–3.85 ma sediment of the Kekeya section at Yecheng, Xinjiang (in Chinese with English abstract). Geological Science and Technology Information 29(4):43–50

Young G, Nesbitt HW (2001) The chemical index of alteration as a palaeoclimatic proxy, new and refined proxies in palaeoceanography and palaeoclimatology. In: Abstracts for EUG XI, theme CC: climate change. Cambridge publications, the conference company, UK, Cambridge, p 108

Yuan D, Cheng H, Edwards RL, Dykoski CA, Kelly MJ, Zhang M, Qing J, Lin Y, Wang Y, Wu J, Dorale JA, An Z, Cai Y (2004) Timing, duration, and transitions of the last interglacial Asian monsoon. Science 304:575–578

Zhao H, Han X, Chen R, Chu F, Gao S (2008) Characteristics of main elements and their palaeoenvironment significance of Core 191 in the northern South China Sea (in Chinese with English abstract). Acta Oceanol Sin 30:85–93

Publisher's Note